NJC

ROYAL SOCIETY OF CHEMISTRY

PAPER

View Article Online
View Journal | View Issue

Cite this: *New J. Chem.*, 2023, **47**, 4543

A structural spectroscopic study of dissociative anaesthetic methoxphenidine†

Bronislav Jurásek, *[ad] Patrik Fagan, [b] Bohumil Dolenský, [b] Natalie Paškanová, [ad] Kristýna Dobšíková, [b] Ivan Raich, [d] Radek Jurok, [ac] Vladimír Setnička, [b] Michal Kohout, [c] Jan Čejka [e] and Martin Kuchař [adf]

Methoxphenidine was originally patented for its properties to treat neurotoxic injury. However, due to its side effects, it failed to become a drug and later reappeared on the black market among so-called new psychoactive substances. Methoxphenidine belongs among dissociative anaesthetics, which came to the forefront of medicinal interest due to their potential for depression treatment. Despite its pharmacological history and black market availability, there is still a lack of pharmacological data on this substance and a shortage of methods enabling further biological studies. To offer tools for psychopharmacological studies of the enantiomers of this compound, we have developed a chiral resolution process by crystallization using a natural pool of chiral substances. We further developed a novel analytical method to control the optical purity of the obtained enantiomers using chiral supercritical fluid chromatography, which represents the contemporary green and sustainable method for chiral separation. To determine the absolute configuration of the crystallized enantiomers, we employed a combination of the electronic circular dichroism spectra supported by quantum chemical calculations. Furthermore, to verify our approach, we analysed the sample by single crystal diffraction. We believe that the tools within our work that enable pharmacological studies focused on both enantiomers of methoxphenidine may be useful not only for medicinal chemists but also for the broader scientific community.

Received 15th December 2022,
Accepted 23rd January 2023

DOI: 10.1039/d2nj06126k

rsc.li/njc

1 Introduction

Designer drugs have been a phenomenon affecting the global drug scene for nearly two decades. The denomination "designer drugs" points to their creation process, which resembles the design of novel substances. These compounds are typically structurally related to already existing drugs of abuse. Each chemical modification of the structure of a psychoactive substance creates a novel one that aims to mimic the effects of the original. Because of the mentioned novelty the as-prepared compounds also evade the legislation. The European Monitoring Centre for Drugs and Drug Addiction (EMCDDA) divides designer drugs (by another name New Psychoactive Substances, NPS) into several groups; one of which is dissociative anaesthetics.[1] Although dissociative anaesthetics are a relatively small group of substances, they are popular among users as recreational drugs. On the other hand, due to the relatively recent discovery that ketamine may be useful for depression treatment, the entire group of dissociative anaesthetics came to the forefront of medicinal interest.[2–4] Regardless of this discovery or the popularity of dissociative anaesthetics, there is often a lack of basic data on their toxicology and pharmacology.

One of the important dissociative anaesthetics is methoxphenidine (2-MeO-diphenidine, MXP), which was originally patented in 1989 as a possible therapeutic for the treatment of neurotoxic injury, however, it did not fulfil the necessary requirements.[5–7] Failing to become a drug, MXP reappeared on the drug market approximately two decades later as a dissociative anaesthetic with significant abusive potential.[7,8] Unlike common dissociative anaesthetics, which bear the arylcyclohexylamine type of structure, MXP belongs to the group of arylethylamines. In experiments in rodents focused on the chronic administration of methoxphenidine, Hur *et al.* observed hyperactivity, increased

[a] *Forensic Laboratory of Biologically Active Substances, University of Chemistry and Technology Prague, Technická 5, 166 28 Prague, Czech Republic. E-mail: jurasekb@vscht.cz*
[b] *Department of Analytical Chemistry, University of Chemistry and Technology Prague, Technická 5, 166 28 Prague, Czech Republic*
[c] *Department of Organic Chemistry, University of Chemistry and Technology Prague, Technická 5, 166 28 Prague, Czech Republic*
[d] *Department of Chemistry of Natural Compounds, University of Chemistry and Technology Prague, Technická 5, 166 28 Prague, Czech Republic*
[e] *Department of Solid State Chemistry, University of Chemistry and Technology Prague, Technická 5, 166 28 Prague, Czech Republic*
[f] *Psychedelic Research Centre, National Institute of Mental Health, Topolová 748, 250 67 Klecany, Czech Republic*

† Electronic supplementary information (ESI) available. CCDC 2195741. For ESI and crystallographic data in CIF or other electronic format see DOI: https://doi.org/10.1039/d2nj06126k

impulsivity, recognition memory dysfunction, social withdrawal, depressive-like behaviour and schizophrenia-relevant symptoms.[9] Compared to controls the MXP treated animals had significantly increased expression levels of CAMK2, DAT (dopamine transporter, SLC6A3), p-DAT, D_1 receptor, and TH and an increase in the p-DAT/DAT ratio. In comparison to its structural analogue diphenidine, MXP is a slightly less potent inhibitor of NET and a significantly less potent inhibitor of DAT.[10,11] According to unofficial user experiences, MXP is less active than common arylcyclohexylamines like methoxetamine, deschloroketamine or ketamine,[12,13] yet it may be quite addictive.[9,14–16] Despite the lower potency, several intoxications were associated with this substance to date.[12,13] Symptoms like rhabdomyolysis, ischemic cerebral disease, acute kidney failure or other serious psychic and somatic complications can also occur during the intoxications.[14,17,18] Some symptoms may be even indistinguishable from those of major psychoses and thus it could be misdiagnosed.[19] Moreover, MXP is sometimes used in combination with other NPS,[20] which further complicates attributing particular effects to the substances. This further exerts pressure on keeping the methods up to date to be able to detect xenobiotics in biological samples. Some approaches were used for MXP detection selectivity of the heat based method combined with molecularly imprinted polymers (MIPs).[21,22] On the other hand, MXP can be detected using HPLC-MS methods either focused on the analyses of a large amount of samples in biological materials,[23] hair[24] or those focused on the separation of specific regioisomers of the MXP.[25–28]

Similar to arylcyclohexylamines, MXP contains a stereogenic centre in its molecular structure. This fact is disregarded by the manufacturers and, therefore, it is present in drug market as a racemic mixture. There are already comprehensive analytical methods aimed at various designer drugs, including MXP, however, only a paucity of them is related to its enantioseparation. This is despite the fact that enantiomers of the majority of drugs differ in effects and toxicity.[29] This is true also for dissociative anaesthetics and, particularly, ketamine;[2] the enantiomerically pure metabolites are being screened because of their high pharmaceutical potential.[30] The resolution and characterization of enantiomers of NPS are therefore of eminent interest not only due to toxicity differences but also due to their pharmaceutical potential.

For chiral separation of MXP, capillary electrophoresis (CE) with cyclodextrins as chiral selectors was used.[31–33] The enantioseparation methods by liquid chromatography and polysaccharide chiral stationary phases were also introduced.[34–37] There is also one method of chiral separation of MXP using supercritical fluid chromatography (SFC) by the vancomycin-based chiral stationary phase.[38] The main advantage of this approach is that SFC offers fast and inexpensive enantioselective methods.[39]

Within our previous work, we discovered that at least some MXP samples on the drug market may contain zinc(II) complexes instead of the chloride anion which we believe may be responsible for some unusual properties of the sample (the longer onset of the compound, lower potency or probably even the reported increase of blood pressure).[40] Within this work, we have developed a chiral resolution by crystallization, which we used to obtain both the enantiomers of MXP. To control the chiral purity of the obtained enantiomers, we used the high performance liquid chromatography-photodiode array detection (HPLC-PDA) method, which offers sufficient enantioseparation parameters.[36] In addition, we also developed a new supercritical fluid chromatography with photodiode array detection (SFC-PDA) to obtain improved chromatographic parameters. The molecular structure of MXP was supported *via* nuclear magnetic resonance (NMR) studies. Finally, a combination of electronic circular dichroism (ECD) spectra supported by the density functional theory (DFT) calculation has been used to assign the absolute configuration of both enantiomers.

2 Experimental

2.1 Materials

LC-MS-grade methanol, ethanol, propan-2-ol, and acetonitrile were supplied by Labicom (Olomouc, Czech Republic). Carbon dioxide 4.8 grade (99.998%) was obtained from SIAD (Prague, Czech Republic). Diethylamine and formic acid (98–100%) were purchased from Sigma Aldrich (Prague, Czech Republic). (+)-2,3-Dibenzoyl-D-tartaric and (−)-2,3-dibenzoyl-L-tartaric acid monohydrates were purchased from Sigma Aldrich (Prague, Czech Republic). Isopropylamine (99%) was purchased from Fluorochem (Hadfield, United Kingdom). Deionized water (UCT Prague) was used for the ECD spectra measurement. A standard of MXP was synthesized in our previous study.[40]

2.2 Crystallization of the enantiomers

Racemic MXP free base (1 eq.) and (−)-2,3-dibenzoyl-L-tartaric acid monohydrate (1 eq.) were dissolved in dichloroethane (DCE) and the resulting MXP salt was crystallized from DCE (dichloroethane offered the best results; in other solvents the solubility of the enantiomers was higher)[41] upon the addition of diethylether (Et_2O). The obtained solid was dissolved in dichloroethane using a heat gun and recrystallized twice by adding Et_2O. The filtered crystals were dissolved in water; the obtained solution was basified using an aqueous NaOH solution and extracted with dichloroethane. The organic phase was dried over anhydrous $MgSO_4$, filtered and evaporated to dryness. The obtained methoxphenidine free base (MXP-a) was dissolved in Et_2O and a 1.1 M solution of HCl in Et_2O was added. The obtained suspension was evaporated to dryness and crystallized from acetone. The obtained MXP-a hydrochloride was obtained as white crystals.

The filtrate obtained from the first crystallization was basified with the aqueous NaOH solution and the organic fraction was separated. The organic phase was dried over anhydrous $MgSO_4$, filtered and evaporated to dryness. The obtained methoxphenidine free base – MXP-b (1 eq.) and (+)-2,3-dibenzoyl-D-tartaric acid monohydrate (1 EQ) was dissolved in DCE and the resulting MXP salt was crystallized from DCE by adding Et_2O. The following workup was the same as for the previous

enantiomer, and MXP-b hydrochloride was obtained as white crystals.

2.3 Instrumentation

HPLC and SFC. An Acquity UltraPerformance Convergence Chromatography™ (UPC^2) system from Waters (Milford, MA, USA) was used. The system featured a binary solvent delivery pump, an autosampler, an automated back-pressure regulator, a column oven compatible with 250 mm length columns, and a photodiode array (PDA) detector. Empower® 3 software (Waters, Milford, MA, USA) was used to control the chromatographic system and acquire data. The data were further evaluated with Microsoft Excel.

A Lux® Cellulose-2 250 × 4.6 mm, 5 μm from Phenomenex (Aschaffenburg, Germany) containing cellulose tris(3-chloro-4-methylphenylcarbamate) and Chiral ART Amylose-C 250 × 4.6 mm, S-5 μm from YMC (Dinslaken, Germany) containing cellulose tris(3,5-dimethylphenylcarbamate) served as chiral stationary phases (CSPs) in HPLC. Alcyon SFC CSP Amylose-SA containing amylose tris(3,5-dimethylphenylcarbamate), Cellulose-SB containing cellulose tris(3,5-dimethylphenylcarbamate) and Cellulose-SC containing cellulose tris(3,5-dichlorolphenylcarbamate) (150 × 4.6 mm, 5 μm) columns from YMC (Dinslaken, Germany) and CHIRALPAK® IE-3 150 × 4.6 mm, 5 μm from CTE Europe (Illkirch, France) containing amylose tris(3,5-dichlorophenylcarbamate) served as CSPs in SFC. The Alcyon SFC CSP Amylose-SA and Chiral ART Amylose-C comprise the same selector.

2.4 Chromatographic conditions

HPLC. The mobile phase is composed of acetonitrile/propan-2-ol/diethylamine/formic acid (95/5/0.1/0.1; v/v/v/v). The flow rate was set to 1 mL min^{-1} for all performed analyses. The temperature was kept at 27 °C. The automatic back pressure regulator (ABPR) was off. The injection volume was 5 μL and the autosampler temperature was set to 10 °C. The void volume was determined using the sample solvent peak. All measurements were performed in duplicate.

SFC. Various volume ratios of CO_2, modifiers and additives were tested for the mobile phase. The chromatographic measurements were performed at a flow rate of 1 mL min^{-1} and a temperature of 35 °C, and the ABPR was set to 2500 psi (172 bar). The PDA was set at wavelengths of 220 and 254 nm for the detection of analytes. All experiments were measured in duplicate during the optimisation. The injection volume was 2 μL and the autosampler temperature was set to 10 °C. The void volume was determined using the sample solvent peak.

2.5 Electronic circular dichroism

The ECD and UV absorption spectra were recorded on a Jasco J-815 spectrometer (Jasco, Japan). All spectra were recorded in the spectral range of 185–330 nm at ambient temperature in a quartz cuvette (Hellma, Germany) with an optical path length of 1 mm. Samples were prepared at a concentration of 1 g L^{-1} for the spectral range of 244–330 nm and 0.03 g L^{-1} for the spectral range of 185–244 nm. The following parameters were set: response time 4 s, scanning speed 50 nm min^{-1}, bandwidth 1 nm, and sensitivity 100 mdeg. The final spectra were obtained by averaging 4 accumulations. The baseline was corrected by subtracting the spectra of the solvent measured under the same experimental conditions.

2.7 DFT calculation

The starting geometries of (*R*)-MXP hydrochloride were determined by systematic changes of 120° rotation of labelled dihedral angles α_1–α_5 (Fig. 1(B)) performed using the MCM

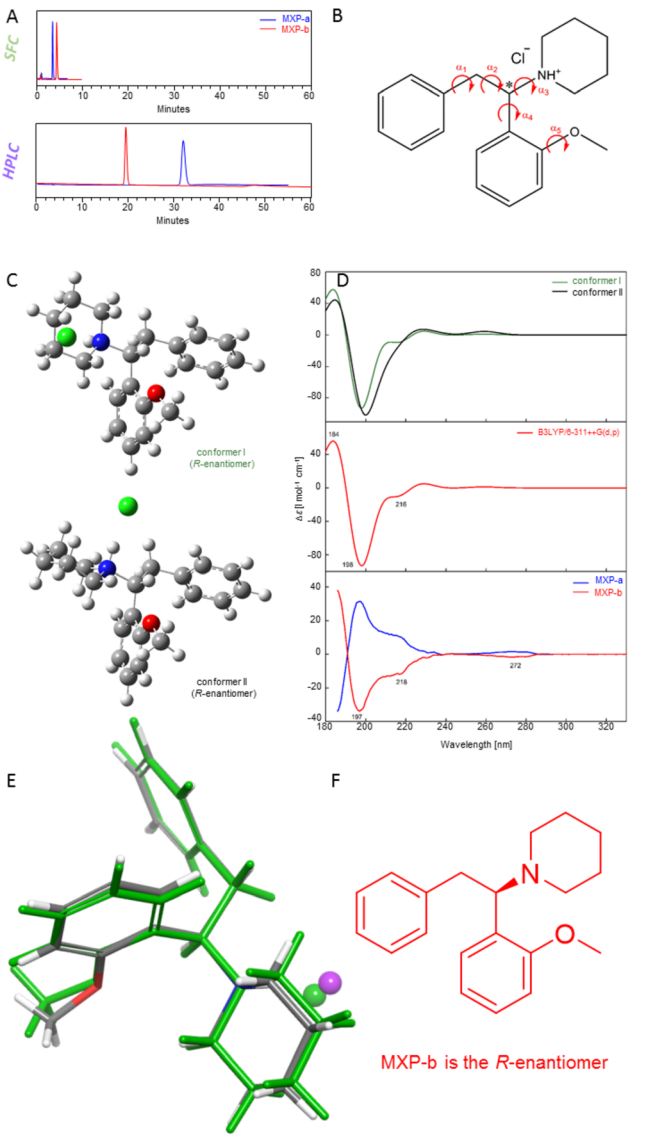

Fig. 1 (A) The SFC and HPLC methods for the enantioseparation of methoxphenidine. (B) Structure of MXP with the chiral centre labelled by an asterisk and five dihedral angles α_1–α_5. (C) The stable conformers of (*R*)-MXP hydrochloride were calculated at the B3LYP/6-311++G(d,p) level. Colors used in the figure: blue – nitrogen, grey – carbon, white – hydrogen, red – oxygen, green – chlorine. (D) The ECD spectra of MXP·HCl. The simulated spectra of individual conformers at the B3LYP/6-311++G(d,p) level (top), their Boltzmann-weighted spectra (middle) and the experimental spectra of both enantiomers (bottom). The spectra were displayed in the spectral range of 185–330 nm. (E) Overlay of the conformer of *R*-MXP found in the crystal using X-ray analysis (grey) and the most stable conformer I predicted by *ab initio* calculations (green). (F) The confirmed absolute structure of *R*-MXP (MXP-b).

software.[42] As a result, 244 starting geometries were obtained. An appropriate position of chlorine ion was achieved by placing the chlorine ion in different positions and distances in relation to the (*R*)-MXP molecule. All geometries were optimized at the B3LYP/6-31G(d) level of theory. Solvation effects were considered involving the conductor-like polarizable continuum solvent model (CPCM).[43] After optimization, and verification using frequency calculations, two stable and populated conformers were obtained for (*R*)-MXP. Those were further reoptimized at the higher levels of theory (B3LYP/6-311++G(d,p), B3PW91/6-311++G(d,p), B3PW91/aug-cc-pVDZ, B3PW91/aug-cc-pVTZ, CAM-B3LYP/6-311++G(d,p)) using the Gaussian 16 program package.[44] Here, only the results with the best conformity with the experimental spectra are presented. The weighted average ECD and UV absorption spectra were simulated based on the Boltzmann distribution using the Gibbs free energy at a temperature of 298 K. For the visualization of ECD and UV spectra, the Gaussian band shape with 10 nm as a half-height width was applied and 50 excited states were calculated.

2.8 Single crystal data collection and evaluation

Data were collected on a Bruker D8 VENTURE system equipped with a Photon II detector, a Cu Kα Incoatec microfocus sealed tube (λ = 1.54178 Å) with a multilayer monochromator and using combined φ and ω scans at 180 K. For more details see Table S3 (ESI†). The positional and anisotropic thermal parameters of all non-hydrogen atoms were refined. All H atoms were located in a difference map, but repositioned geometrically; then they were initially refined with soft restraints on the bond lengths and angles to regularize their geometry (C–H in the range of 0.93–0.98 Å, N–H set to 0.86 Å and O–H to 0.82 Å) and U_{iso}(H) (in the range 1.2–1.5 times U_{eq} of the parent atom), after which the positions of carbon bound hydrogen atoms were refined with riding constraints. The same isotropic soft restraints were used during the final stages of the refinement when the positional parameters of the hetero-bound hydrogen atoms were refined. No solvent-accessible voids were found in the structure. The absolute configuration was unambiguously assigned according to the refinement of Flack's parameter to the final value of $x = -0.012(10)$. The data were included in the Cambridge Crystallographic Data Centre (CCDC) under the number 2195741.†

Data collection: APEX4 v2019 (Bruker AXS);[45] unit cell refinement: SAINT V8.40B (Bruker AXS Inc., 2019); data reduction: SAINT (Bruker AXS Inc., 2019);[45] the program used to solve the structure: SIR92 (Altomare *et al.*, 1994);[46] the program used to refine the structure: CRYSTALS.[47]

2.9 NMR spectroscopy

NMR spectra were recorded using a 500 MHz ECZ 500R instrument (JEOL, Tokyo, Japan) at various temperatures. The chemical shifts (δ) are presented in ppm, and the coupling constants (J) are presented in Hz. The ^{1}H and ^{13}C chemical shifts are referenced to tetramethylsilane using the solvent signals C**H**D$_2$SOCD$_3$ 2.50 ppm, **C**D$_3$SOCD$_3$ 39.52 ppm, or the signal of the deuterium lock when measured in D$_2$O. The signal assignments were done using standard 1D and 2D NMR experiments.

3 Results and discussion

A standard of MXP was enantiomerically resolved using crystallization with appropriate 2,3-dibenzoyl-tartaric acid enantiomers. To control and confirm the optical purity during and after the crystallization processes, we needed a fast method for the chiral resolution of the original racemic mixture. For this purpose, we employed a HPLC method published by M. Taschwer *et al.*[36] (results can be found in the ESI† (Fig. S1 and S2)). Although this analytical method was suitable for our purpose, it was rather time-consuming, required long column equilibration and, therefore, produced a substantial amount of organic waste. One of the possibilities to mitigate these issues is to develop a method for the chiral resolution of MXP in supercritical fluid chromatography (SFC). SFC typically offers shorter method times due to the higher diffusivity of the mobile phase as well as the higher flow rates while using carbon dioxide as the bulk mobile phase, thereby producing much less toxic waste than HPLC analysis.

3.1 Optimization of SFC enantioseparation

Based on published data obtained from chiral separation in the HPLC mode, four polysaccharide stationary phases (Alcyon SFC CSP Amylose-SA, Cellulose-SB and Cellulose-SC and CHIRALPAK® IE-3) were chosen for the optimization of enantioseparation of MXP under SFC conditions. To facilitate fast elution of the sample from the stationary phase, polar organic modifiers (propan-2-ol, ethanol, methanol and acetonitrile) were introduced into the bulk supercritical carbon dioxide mobile phase. Polar organic modifiers are added to the CO_2 mobile phase in order to elute analytes of moderate to high polarity. Carbon dioxide possesses high miscibility with organic solvents with a wide polarity range, which brings some unique characteristics to SFC, especially a broad operational window to tune (enantio)selectivity. However, the supercritical state of CO_2 is shifted to higher temperature and pressure figures by adding a polar modifier. The term SFC is typically used for all sub-regions, such as subcritical fluid chromatography of enhanced-fluidity liquid chromatography.[48–50] Recently, the term unified chromatography is used for SFC separations performed over the whole concentration range of a modifier.[51]

To suppress possible non-enantioselective interaction of the analyte with the stationary phase (*e.g.*, residual silanol groups on the silica surface), basic (isopropylamine, diethylamine) and acidic (formic acid) additives to the mobile phase were screened. All the results from the optimization can be found in the ESI† (Fig. S3).

Effects of the modifiers on the enantioseparation. The ratio of CO_2, modifier and additives was set up at 90/10/0.1 (v/v/v) as default. A mobile phase containing an acetonitrile modificator allowed only partial enantioseparation on Cellulose-SB and CHIRALPAK® IE-3. More significant results were observed for

alcohol modifiers. The retention increased with a decrease in the molecular weight of alcohols with added basic additives. On the other hand, the resolution decreased with a decrease in the molecular weight of alcohols with added basic additives, and therefore, propan-2-ol was selected as the best modifier for the analysis of MXP. The strongest impact of this trend was observed on CHIRALPAK® IE-3 (Table 1). Of the applied alcohol modifiers, propan-2-ol is the most lipophilic one which leads to higher solubility of the MXP in the mobile phase and lower adsorption on the CSP. On the other hand, it is less polar which seems to play a crucial role in the observed chiral resolution.

Effects of additives on enantioseparation. In general, the use of acidic additives was not effective, and there was practically no elution in 150 minutes. The basic additives caused the elution of analytes on all columns. While diethylamine is the most common additive used for enantioseparation by HPLC, our experience suggests that isopropylamine could significantly enhance enantioselectivity and resolution under SFC conditions. On the other hand, the combination of formic acid with basic additives showed the opposite effect than was observed for pure basic additives. The retention decreased with a decrease in the molecular weight of alcohols. This trend was again most pronounced for column CHIRALPAK® IE-3 (Table 1).

CSPs. The best conditions for the chiral resolution of MXP differed for the selected CSPs (for the full set of data from chromatographic screening) (see Table S1 in the ESI†). The highest resolution (R = 12.86) was observed on an Alcyon SFC CSP Amylose-SA column with the composition of the mobile phase as follows: CO_2/propan-2-ol/diethylamine/formic acid (90/10/0.1/0.1, v/v/v/v). The resolution of R = 3.78 was achieved on a CHIRALPAK® IE-3 column with the composition of the mobile phase as follows: CO_2/propan-2-ol/isopropylamine (90/10/0.1, v/v/v) while it was R = 2.73 on an Alcyon SFC CSP Cellulose-SC column with the composition of the mobile phase as follows: CO_2/ethanol/diethylamine (90/10/0.1, v/v/v). There was only one result of enantioseparation for an Alcyon SFC CSP Cellulose-SB column with resolution R = 1.05 with the composition of the mobile phase as follows: CO_2/acetonitrile/diethylamine/formic acid (90/10/0.1/0.1, v/v/v/v).

Based on the results of this initial screening, two CSPs, namely Alcyon SFC Amylose-SA and CHIRALPAK® IE-3, were selected for further optimization of the chiral separation method. We have focused on the utilization of propan-2-ol, diethylamine and formic acid on an Alcyon SFC CSP Amylose-SA column. A higher amount of modifiers with additives led to a significant decrease of retention times. Selectivity and resolution were highest at the composition of the mobile phase 80/20/0.1/0.1 and then they fell again. Despite the best results being achieved for the mobile phase containing CO_2/propan-2-ol/diethylamine/formic acid (90/10/0.1/0.1, v/v/v/v), an additional increase in the modifier concentration was not possible due to elution of one enantiomer in the void volume.

Using a CHIRALPAK® IE-3 column we investigated also a different ratio of CO_2 and propan-2-ol with isopropylamine. Similar to the previous case, the retention distinctly decreased with an increase in the amount of alcohol, while both the selectivity and resolution values increased. Thanks to that, we were able to resolve the enantiomers of MXP in five minutes using a CHIRALPAK® IE-3 column and the mobile phase CO_2/propan-2-ol/isopropylamine (60/40/0.1, v/v/v). The retention times of the enantiomers of MXP were t_1 = 3.19 and t_2 = 4.29 with an excellent resolution factor of 5.26 (Table 2).

Repeatability. The improved CO_2/modifier pumping system and backpressure regulation features of the UPC^2 instrumentation allow for improved flow and backpressure control in comparison to previous SFC instruments. This in turn leads to highly reproducible retention, which is documented by the retention time as well as the resolution factor repeatability (Table 3). Intra- and interday repeatability provided RSD values in the ranges 0.08–2.26 for retention times.

3.2 Enantiomeric purity of methoxphenidine

We employed our newly developed method using a CHIRALPAK® IE-3 column with a mobile phase composed of CO_2/

Table 1 Effect of four modifiers on the elution time (t_1, t_2), selectivity (α) and resolution (R); ''×'' means no elution in 150 minutes, ''—'' means no chiral separation

CHIRALPAK® IE-3									
MP	t_1 [min]	t_2 [min]	α	R	MP	t_1 [min]	t_2 [min]	α	R
CO_2/propan-2-ol/isopropylamine (v/v/v)					CO_2/ethanol/isopropylamine (v/v/v)				
90/10/0.1	**20.38**	**31.92**	**1.59**	**3.78**	90/10/0.1	41.70	49.90	1.20	2.30
CO_2/propan-2-ol/diethylamine (v/v/v)					CO_2/ethanol/diethylamine (v/v/v)				
90/10/0.1	18.06	25.02	1.40	2.74	90/10/0.1	36.05	43.60	2.95	
CO_2/propan-2-ol/formic acid (v/v/v)					CO_2/ethanol/formic acid (v/v/v)				
90/10/0.1	×	×	×	×	90/10/0.1	11.50	—	—	—
CO_2/propan-2-ol/diethylamine/formic acid (v/v/v/v)					CO_2/ethanol/diethylamine/formic acid (v/v/v/v)				
90/10/0.1/0.1	118.32	133.29	1.13	1.70	90/10/0.1/0.1	82.73	94.53	1.14	2.34
CO_2/methanol/isopropylamine (v/v/v)					CO_2/acetonitrile/isopropylamine (v/v/v)				
90/10/0.1	54.08	61.06	1.13	1.63	90/10/0.1	10.67	12.63	1.20	0.77
CO_2/methanol/diethylamine (v/v/v)					CO_2/acetonitrile/diethylamine (v/v/v)				
90/10/0.1	56.38	62.48	1.11	1.67	90/10/0.1	5.89	6.48	1.11	—
CO_2/methanol/formic acid (v/v/v)					CO_2/acetonitrile/formic acid (v/v/v)				
90/10/0.1	×	×	×	×	90/10/0.1	×	×	×	×
CO_2/methanol/diethylamine/formic acid (v/v/v/v)					CO_2/acetonitrile/diethylamine/formic acid (v/v/v/v)				
90/10/0.1/0.1	76.07	76.12	1.09	1.48	90/10/0.1/0.1	×	×	×	×

Table 2 Effect of different ratios of CO_2/modifier on the elution time (t_1, t_2), selectivity (α) and resolution (R)

CHIRALPAK® IE-3				
MP	t_1 [min]	t_2 [min]	α	R
CO_2/propan-2-ol/isopropylamine (v/v/v)				
60/40/0.1	3.19	4.59	1.53	5.26
70/30/0.1	5.13	6.82	1.39	3.35
80/20/0.1	9.53	12.51	1.34	2.81
90/10/0.1	20.38	31.92	1.59	3.78

propan-2-ol/isopropylamine (60/40/0.1, v/v/v). In this case, the first eluted peak was MXP-a, and the second one is MXP-b. The final purity of enantiomers was determined from the ratio of peak area (Fig. S1–S3, ESI†). The enantiomeric purity of MXP-a was 99.63% (99.26% ee (enantiomeric excess)) and that of MXP-b was 99.85% (99.7% ee).

3.3 The comparison of SFC and HPLC methods of enantioseparation

In comparison, shorter retention times, a more stable baseline and a higher detector response were achieved (see Fig. S4 in the ESI†) thanks to the new SFC method (Fig. 1(A)). The higher response of the detector in SFC is primarily caused by shorter retention times leading to significantly better peak shapes than for the HPLC method. The resolution is lower than the resolution achieved under HPLC conditions; however, it is still more than sufficient. Because of the composition of the mobile phase (CO_2/propan-2-ol/isopropylamine), the method is compatible with a mass spectrometer allowing for future applications.

The enantiomer elution order (EEO) under SFC conditions was reversed in comparison to the method published by Taschwer (see ESI,† Fig. S1). The reversal of elution order can be achieved in several ways, typically by changing the CPS for its enantiomeric variant (for brush-type CSPs),[52] or *via* utilizing structurally modified selectors.[53] However, a change in chromatographic conditions can be sufficient to trigger the EEO as well.[54] Recently, it has been shown that the EEO in various chromatographic modes strongly depends on the amount of a polar co-solvent in the bulk mobile phase.[55] Therefore, it is assumed that in this study, the EEO reversal is caused by the higher content of the polar modifier in the subcritical mobile phase. To ascertain the absolute configuration of the obtained enantiomers, we employed the combination of density functional theory calculations with circular dichroism measurements.

3.4 Conformational analysis

The most starting structures converged to the same geometry or the relative abundance of different geometries was too low.

Table 4 The two stable conformers of (*R*)-MXP hydrochloride with their dihedral angles, relative Gibbs free energies and relative abundances simulated at the B3LYP/6-311++G(d,p) level

Conformer	α_1	α_2	α_3	α_4	α_5	ΔG_{DFT} [kJ mol^{-1}]	Relative abundance [%]
I	−73	162	−171	−46	−178	0	92
II	−75	171	−66	−57	−179	6.2	8

As the result, we obtained two stable conformers (Fig. 1(C)) for (*R*)-MXP hydrochloride. The revealed stable conformers were reoptimized at the higher level of theory B3LYP/6-311++G(d,p) and their relative abundances were calculated based on Boltzmann distribution (Table 4). Structural parameters were similar except for the dihedral angle α_3, for which we observed the difference ∼−105° (Fig. 1(C) and Table 4). The orientation of the piperidine ring had the highest effect on the stability of the structure.

Electronic circular dichroism and ultraviolet absorption spectroscopy. The mirror symmetry pattern of the experimental ECD spectra of MXP hydrochloride (Fig. 1(D) bottom) indicated their enantiomeric character. Based on very good agreement between the experimental (Fig. 1(D) bottom) and Boltzmann weighted spectrum of (*R*)-MXP (Fig. 1(D) middle), the absolute configuration of MXP-b was determined as the (*R*)-enantiomer. All observed spectral bands and their maxima were correctly predicted in the Boltzmann weighted spectrum (Fig. 1(D) middle). In the experimental spectrum of MXP hydrochloride, bands were observed at 185, 197, 218 and 272 nm (Table 5) reflecting the combination of the electronic transitions. Band 4 occurred at 272 nm in the experimental spectrum; it was present only in the spectrum of conformer II and, due to its low relative abundance, it did not appear in the Boltzmann weighted spectrum. The band located at 218 nm was correctly predicted only in the simulated spectrum of conformer I. Band 4 was mainly an expression of electronic transitions from the highest occupied molecular orbital (HOMO, Fig. S7, ESI† left) to the lowest unoccupied molecular orbital (LUMO, Fig. S7, ESI† right).

In the experimental spectra of both MXP enantiomers, two bands were found (198 nm and 277 nm, Fig. 1(D) bottom). The broad band located at 277 nm in the experimental spectrum was found redshifted by 26 nm in the Boltzmann-weighted spectrum (Fig. 1(D) middle, Table 5). The band shoulder at 198 nm was found in the experimental spectrum of MXP hydrochloride and was included in the broad band 1 in both simulated spectra of individual conformers.

Nuclear magnetic resonance spectroscopy. The ^{13}C NMR spectrum of MXP free base is simple since the fast inversion of nitrogen configuration (Fig. S8, ESI†) leads to a single sharp

Table 3 A method validation with regard to repeatability of the elution time (t_1, t_2), selectivity (α) and resolution (R)

Repeatability		t_1 [min]	±	RSD	t_2 [min]	±	RSD	α	±	RSD	R	±	RSD
Intraday	n = 6	3.24	0.00	0.08	4.53	0.00	0.11	1.53	0.00	0.04	5.55	0.08	1.47
Interday	n = 12	3.29	0.07	2.26	4.56	0.05	1.16	1.51	0.02	1.56	5.33	0.32	5.94

Table 5 Experimental and B3LYP/6-311++G(d,p) simulated wavelengths for the ECD spectra of (*R*)-MXP hydrochloride

Band number	Experimental spectrum [nm]	Band sign	Simulated spectrum [nm]	Band sign
1	185	+	184	+
2	197	−	198	−
3	218	−	216	−
4	272	−	−	×

signal for diastereotopic carbon atoms $C3_S$ and $C3_R$, and a single sharp signal for diastereotopic carbon atoms $C4_S$ and $C4_R$. Indeed, all ^{13}C signals of MXP free base are sharp,[6] which means there are no chemical exchanges of medium rate on the NMR time scale.

In contrast, the ^{13}C NMR spectrum of MXP·HCl contains a few oddities. At first, as the protonation of nitrogen dramatically slowed the rate of its configuration inversion, the signals of $C3_S$ and $C3_R$, and signals of $C4_S$ and $C4_R$ are not averaged. Hence, four signals at 51.89, 48.81, 22.52 and 22.48 ppm were observed in DMSO-d_6 solution by 600 MHz NMR instrument (^{13}C at 151 MHz).[6] Our measurement in DMSO-d_6 solution at 22 °C by 500 MHz NMR instrument (^{13}C at 126 MHz) gave two signals at 51.809 and 48.317 ppm for C3 carbons, however only one broad signal at 22.450 ppm for C4 carbons as the result of the lower coalescence temperature at the lower magnetic field. Our measurement in D_2O solution at 22 °C gave two signals at 52.533 and 50.918 ppm for C3 carbons ($\Delta\nu$ = 203.1 Hz), which coalesced approximately at 75 °C, and two signals at 22.962 and 22.739 ppm for C4 carbons ($\Delta\nu$ = 28.0 Hz), which coalesced approximately at 40 °C (see the ESI†). In the second, both in D_2O and DMSO-d_6 solutions we observed very broad signals of carbon C1. Due to proximity, we suggest it is the consequence of the nitrogen inversion and/or NH dissociation. In the third, both in D_2O and DMSO-d_6 solutions, in the aromatic part of the NMR spectrum, we observed a broad signal exclusively for carbon C11. Since there is no such broadening of any ^{13}C signal in the MXP free base spectrum, the nitrogen protonation is the origin obviously. We deduced it could be a consequence of the hindered rotation of the methoxyphenyl group (*vide infra*).

The ^1H NMR spectrum of the MXP free base exhibited a single sharp quintet for hydrogen C5 of piperidine both in $CDCl_3$[6] and CD_3OD, which is the consequence of fast piperidine ring conformation changes on the NMR time scale (note that the nitrogen inversion is not necessary). The signals of the hydrogen atoms at C3 and C4 carbons are rather complex since they are diastereotopic, and hence second order signals are observed. The peaks of the multiplet signals of the hydrogen atoms at the C4 carbons are sharp, which confirms the fast chemical changes. The peaks of the multiplet signals of the hydrogen atoms at C3 carbons are broader, which can be the consequence of a tiny long range coupling, a protonation equilibrium on the nitrogen due to an impurity, or the mere proximity of the nitrogen atom. The geminal coupling between $H2_R$–$H2_S$ is 13.4 Hz, and the vicinal ones between H1–$H2_R$ and H1–$H2_S$ are 9.2 and 5.7 Hz in $CDCl_3$,[6] and 13.1, 11.0 and 4.3 Hz in CD_3OD. Since the solvent effect on the value of a coupling constant is negligible in general, the differences in J values should be a consequence of the different contents of rotamers and/or their conformations (note that the effect of an impurity cannot be excluded).

In contrast, as expected based on the ^{13}C NMR spectra, the ^1H NMR spectrum of MXP·HCl in D_2O solution confirmed the slow nitrogen inversion; however, slow piperidine ring conformation changes are observed, which are exhibited by observation of ten broad signals for the ten hydrogen atoms of piperidine. Based on the observed correlations in 2D COSY and HSQC spectra we assigned ^1H signals to ^{13}C signals. Based on the multiplicity of the ^1H signals, we estimated which signals are for axial or equatorial hydrogen atoms; in spite of the signals' broadness the couplings of $J > 10$ Hz corresponding to $J_{ax,ax}$ or J_{gem} are well recognized. Based on 2D ROESY spectra we assigned pairs of ^1H signals in chemical exchanges, *i.e.*, $H3_R^{ax}$ – $H3_S^{eq}$, $H3_R^{eq}$ – $H3_S^{ax}$, $H4_R^{ax}$ – $H4_S^{eq}$, $H4_R^{eq}$ – $H4_S^{ax}$, and $H5_Z^{ax}$ – $H5_E^{eq}$. Since the exchanges are observed between the axial and equatorial hydrogen atoms of diastereotopic carbon atoms, the nitrogen inversion, the change of the chair conformation, and a rotation of piperidine have to take place at once. The signals coalesced at high temperatures (see the ESI†).

In accord with the ^{13}C NMR spectra, we observed broad signals for H1 and H11, which are going to be sharp at a higher temperature. Based on the inspection of the physical model of the $MXP{\cdot}H^+$ molecule, and based on the correlation between proton and carbon nuclei in 2D COSY, HSQC, HMBC, NOESY and ROESY NMR spectra we assigned all ^1H and ^{13}C signals and derived the average conformation of $MXP{\cdot}H^+$ (see the ESI†). That is supported by the higher coupling constant H1–$H2_R$ (11.9 Hz) than H1–$H2_S$ (4.4 Hz), by the NOE between H1–$H2_S$ and no H1–$H2_R$, and by the NOE between H11–H1 and H11–$H2_R$ but no H11–$H2_S$. The later NOEs suggest there is a rotation of the methoxyphenyl group, which, based on the molecular model, can be slowed by the formation of the intramolecular hydrogen bond between NH and OMe groups. That can be the origin of the broadness of H1, H11 and C11 signals. Note that interaction with the chloride ion could also play a role.

The strong NOE between $H2_S$ and the broad doublet (equatorial hydrogen) at 3.784 ppm, and significant NOE between H11 and the broad triplet (axial hydrogen) at 2.686 ppm suggest there is no fast rotation of the piperidine group around the C1–N bond, and the configuration of H1 and NH hydrogen atoms is anti-clinal to anti-periplanar. Hence, these signals can be assigned to $H3_S^{eq}$ and $H3_R^{ax}$, respectively, and the resting signals of the piperidine ring can be assigned routinely.

The ^1H NMR spectrum of MXP·HCl in DMSO-d_6 solution suggests that the average conformation at C1–C2 is similar since the coupling constants H1–$H2_R$ (12.1 Hz) than H1–$H2_S$ (3.7 Hz) are similar to the ones in D_2O (*vide supra*). The signals of the hydrogen nuclei on C1 and C3 carbons have additional splitting by hydrogen at nitrogen, which confirms that the dissociation of NH hydrogen is slow at the NMR time scale. The coupling constant of NH to H1 (5.0 Hz) is much less than the ones to $H3_S$ and $H3_R$ (9.6 and 8.9 Hz) having the anti-

periplanar conformation, that suggests the conformation of NH and H1 is not anti-periplanar and/or there is a rotation around C1–N bond. In addition, the coalescence of ^{1}H signals of the piperidine hydrogen atoms takes place at least 50 °C higher than in D_2O (see the ESI†), which can be the consequence of the lower content of proton (deuteron) in DMSO-d_6, which probably affect the rate of the observed changes.

It is worth noting that, to the best of our knowledge, the slowdown of the nitrogen inversion after its protonation, which leads to more complex signals in NMR spectra, is usually omitted in the literature. As another example, we attached the spectra of procaine hydrochloride (see the ESI†). All mentioned ambiguities will be the subject of our next research.

3.5 Single crystal data

Lastly, during the crystallization process, we managed to obtain a single crystal, which we measured by Single Crystal X-Ray Diffraction (see ESI†). The obtained conformation of the *R*-enantiomer was in very good agreement with the simulated data (see the structure overlap in Fig. 1(E)), with an RMS deviation for all heavy atoms of 0.2568 Å. And thus, we conclusively assigned the absolute configuration of the MXP enantiomers (see Fig. 1(F)).

4 Conclusion

The present contribution aimed to develop an enantioseparation method for MXP using SFC and offer a comparison of four commercial CSPs. We have evaluated four polysaccharide-based CSPs (Alcyon SFC CSP Amylose-SA, Cellulose-SB and Cellulose-SC and CHIRALPAK® IE-3) and CO_2-containing mobile phases to improve the efficiency of the existing chiral HPLC method. In comparison, the SFC assay provides a significant decrease in the retention time while maintaining excellent resolution. The repeatability of the method was proven by an intra- and interday validation concerning the retention time and resolution factor. Following the analytical method, a detailed structural analysis of (*R*)-MXP hydrochloride was performed using DFT calculations. As a result, two stable conformers were found in solution, their relative abundances were calculated based on Boltzmann distribution and Boltzmann-weighted spectra were simulated. Their comparison allowed us to determine the absolute configuration and describe revealed stable conformers in detail. Finally, we managed to obtain single crystal data, which were in accordance with the *in silico* calculated results. Based on our knowledge we present for the first time a chiral resolution of MXP by crystallization and the assignment of enantiomer absolute configurations using single crystal data and a combination of CD spectra supported by DFT calculations. In addition, we also present a novel method for the chiral resolution of MXP in SFC by polysaccharide stationary phases.

Author contributions

Conceptualization: B. J.; validation: M. K., V. S. and M. K.; original draft preparation: B. J., B. D., K. D., N. P. and P. F.; project administration: M. K.; funding acquisition: M. K.; HPLC analyses and SFC method development and analyses: N. P; single crystal diffraction: J. Č.; crystallization: R. J.; ECD measurement: K. D.; and DFT calculations: P. F. and I. R. All authors have read and agreed to the published version of the manuscript.

Conflicts of interest

There are no conflicts of interest to declare.

Acknowledgements

This work was supported by the grants of Specific university research – grant no. A2_FPBT_2022_023, by the grant ''Elemental characterization of microtraces and narcotic and psychoactive substances by nuclear analytical methods'' (VI20192022162) and by the Czech Science Foundation (project no. 21-31139J). Computational resources were supplied by the project ''e-Infrastruktura CZ'' (e-INFRA CZ LM2018140) supported by the Ministry of Education, Youth and Sports of the Czech Republic.

References

1 European Monitoring Centre for Drugs and Drug Addiction and Europol, EU Drug Markets Report 2019, Luxembourg, 2019.
2 P. Zanos, R. Moaddel, P. J. Morris, L. M. Riggs, J. N. Highland, P. Georgiou, E. F. R. Pereira, E. X. Albuquerque, C. J. Thomas, C. A. Zarate and T. D. Gould, *Pharmacol. Rev.*, 2018, **70**, 621–660.
3 P. Zanos and T. D. Gould, *Mol. Psychiatry*, 2018, **23**, 801–811.
4 E. Dolgin, *Nat. Med.*, 2013, **19**, 8.
5 N. M. Gray and B. K. Cheng. 1,2-Diarylethylamines for treatment of neurotoxic injury. EP346791, 1989.
6 G. McLaughlin, N. Morris, P. V. Kavanagh, J. D. Power, J. O'Brien, B. Talbot, S. P. Elliott, J. Wallach, K. Hoang, H. Morris and S. D. Brandt, *Drug Test. Anal.*, 2016, **8**, 98–109.
7 A. Helander, O. Beck and M. Bäckberg, *Clin. Toxicol.*, 2015, **53**, 446–453.
8 J. Wallach, H. Kang, T. Colestock, H. Morris, Z. A. Bortolotto, G. L. Collingridge, D. Lodge, A. L. Halberstadt, S. D. Brandt and A. Adejare, *PLoS One*, 2016, **11**, e0157021.
9 K. Hur, S. Kim, S. Ma, B. Lee, Y. Ko, J. Seo, S. Kim, Y. Kim, S. Sung, Y. Lee, Y. H. Jung, Y. Lee, S. Lee and C. Jang, *Br. J. Pharmacol.*, 2021, **178**, 3869–3887.
10 D. Luethi, M. C. Hoener and M. E. Liechti, *Eur. J. Pharmacol.*, 2018, **819**, 242–247.
11 M. Sahai, C. Davidson, N. Dutta and J. Opacka-Juffry, *Brain Sci.*, 2018, **8**, 63.
12 S. P. Elliott, S. D. Brandt, J. Wallach, H. Morris and P. V. Kavanagh, *J. Anal. Toxicol.*, 2015, **39**, 287–293.
13 World Health Organization. Critical Review Report: 2-MEO-Diphenidine 2-MXP, Geneva, 2020.
14 C. Eiden, S. Leone-Burgos, A. Serre, L. Carton, M. Gerardin, R. Le Boisselier, V. Gibaja, E. Monzon, N. Fouilhe,

A. Boucher and H. Peyriere, *Fundam. Clin. Pharmacol.*, 2018, **32**, 654–662.
15 W. Champeau, C. Eiden, J. Gambier and H. Peyriere, *J. Clin. Psychopharmacol.*, 2017, **37**, 376–377.
16 F. Schifano, S. Chiappini, A. Miuli, J. M. Corkery, N. Scherbaum, F. Napoletano, D. Arillotta, C. Zangani, V. Catalani, A. Vento, M. Pettorruso, G. Martinotti, D. G. Massimo and A. Guirguis, *Exp. Neurol.*, 2021, **339**, 113638.
17 R. P. K. Lam, W. L. Yip, M. S. H. Tsui, S. W. Ng, C. K. Ching and T. W. L. Mak, *Clin. Toxicol.*, 2016, **54**, 464–465.
18 A. Valli, D. Lonati, C. A. Locatelli, E. Buscaglia, M. Di Tuccio and P. Papa, *Clin. Toxicol.*, 2017, **55**, 611–612.
19 M. Caloro, G. Calabrò, E. de Pisa, E. Rosini, G. D. Kotzalidis, D. Lonati, C. A. Locatelli, P. Papa, F. Schifano and P. Girardi, *J. Addict. Med.*, 2018, **12**, 247–251.
20 S. P. Elliott, T. Burke and C. Smith, *J. Forensic Sci.*, 2017, **62**, 169–173.
21 J. W. Lowdon, K. Eersels, R. Rogosic, T. Boonen, B. Heidt, H. Diliën, B. van Grinsven and T. J. Cleij, *Sens. Actuators, A*, 2019, **295**, 586–595.
22 R. Rogosic, J. W. Lowdon, B. Heidt, H. Diliën, K. Eersels, B. Van Grinsven and T. J. Cleij, *Phys. Status Solidi*, 2019, **216**, 1800941.
23 J. Czarny, J. Musiał, J. Powierska-Czarny, N. Galant, M. Raczkowski, B. Buszewski and R. Gadzała-Kopciuch, *Microchem. J.*, 2022, **182**, 107922.
24 R. Goncalves, N. Castaing, K. Titier and V. Dumestre-Toulet, *J. Anal. Toxicol.*, 2022, **46**, 328–336.
25 B. O. Boateng, M. Fever, D. Edwards, P. Petersson, M. R. Euerby and O. B. Sutcliffe, *J. Pharm. Biomed. Anal.*, 2018, **153**, 238–247.
26 P. M. Geyer, M. C. Hulme, J. P. B. Irving, P. D. Thompson, R. N. Ashton, R. J. Lee, L. Johnson, J. Marron, C. E. Banks and O. B. Sutcliffe, *Anal. Bioanal. Chem.*, 2016, **408**, 8467–8481.
27 J. K. Field, C. Hinz, C. M. Titman, M. C. Hulme, R. M. Cowan, J. B. Ainsworth-McMillan, N. Gilbert, R. J. Lee, J. Marron, A. Costello, R. E. Mewis, M. R. Euerby and O. B. Sutcliffe, *J. Pharm. Biomed. Anal.*, 2022, **216**, 114798.
28 G. Cochrane, J. K. Field, M. C. Hulme, N. Gilbert, R. E. Mewis, M. R. Euerby and O. B. Sutcliffe, *J. Pharm. Biomed. Anal.*, 2022, **216**, 114797.
29 S. W. Smith, *Toxicol. Sci*, 2009, **110**, 4–30.
30 K. Štefková-Mazochová, H. Danda, W. Dehaen, B. Jurásek, K. Šíchová, N. Pinterová-Leca, V. Mazoch, B. H. Krausová, B. Kysilov, T. Smejkalová, L. Vyklický, M. Kohout, K. Hájková, D. Svozil, R. R. Horsley, M. Kuchař and T. Páleníček, *Br. J. Pharmacol.*, 2022, **179**, 65–83.
31 J. S. Hägele, E. Hubner and M. G. Schmid, *Chirality*, 2020, **32**, 1191–1207.
32 M. Taschwer, M. G. Hofer and M. G. Schmid, *Electrophoresis*, 2014, **35**, 2793–2799.
33 E.-M. Hubner, P. Steinkellner and M. G. Schmid, *J. Pharm. Biopharm. Res.*, 2022, **3**, 187–205.
34 K. Kadkhodaei, M. Kadisch and M. G. Schmid, *Chirality*, 2020, **32**, 42–52.
35 K. Kadkhodaei, L. Forcher and M. G. Schmid, *J. Sep. Sci.*, 2018, **41**, 1274–1286.
36 M. Taschwer, J. Grascher and M. G. Schmid, *Forensic Sci. Int.*, 2017, **270**, 232–240.
37 J. S. Hägele, E. Seibert and M. G. Schmid, *Chromatographia*, 2020, **83**, 321–329.
38 D. Folprechtová, K. Kalíková, K. Kadkhodaei, C. Reiterer, D. W. Armstrong, E. Tesařová and M. G. Schmid, *J. Chromatogr. A*, 2021, **1637**, 461846.
39 G. M. Fassauer, R. Hofstetter, M. Hasan, S. Oswald, C. Modeß, W. Siegmund and A. Link, *J. Pharm. Biomed. Anal.*, 2017, **146**, 410–419.
40 B. Jurásek, S. Rimpelová, M. Babor, J. Čejka, V. Bartůněk and M. Kuchař, *Int. J. Mol. Sci.*, 2022, **23**, 2083.
41 D. Prat, A. Wells, J. Hayler, H. Sneddon, C. R. McElroy, S. Abou-Shehada and P. J. Dunn, *Green Chem.*, 2016, **18**, 288–296.
42 P. Bouř and P. Maloň, *The MCM program*, Prague, Czech Republic, 2021, 1995–2009.
43 V. Barone and M. Cossi, *J. Phys. Chem. A*, 1998, **102**, 1995–2001.
44 M. Frisch, G. Trucks and H. Schlegel, *Gaussian 09.*, Wallingford, United Kingdom, 2009.
45 *B. A. Inc. APEX3*, Saint. Madison, Wisconsin, USA, 2015.
46 A. Altomare, G. Cascarano, C. Giacovazzo, A. Guagliardi, M. C. Burla, G. Polidori and M. Camalli, *J. Appl. Crystallogr.*, 1994, **27**, 435.
47 P. W. Betteridge, J. R. Carruthers, R. I. Cooper, K. Prout and D. J. Watkin, *J. Appl. Crystallogr.*, 2003, **36**, 1487.
48 R. Bennett, M. Biba, J. Liu, I. A. Haidar Ahmad, M. B. Hicks and E. L. Regalado, *J. Chromatogr. A*, 2019, **1595**, 190–198.
49 D. Wolrab, P. Frühauf, C. Gerner, M. Kohout and W. Lindner, *J. Chromatogr. A*, 2017, **1517**, 165–175.
50 D. P. Poe, D. Veit, M. Ranger, K. Kaczmarski, A. Tarafder and G. Guiochon, *J. Chromatogr. A*, 2014, **1323**, 143–156.
51 A. Raimbault, M. Dorebska and C. West, *Anal. Bioanal. Chem.*, 2019, **411**, 4909–4917.
52 J. Herciková, D. Spálovská, P. Frühauf, P. Izák, W. Lindner and M. Kohout, *J. Sep. Sci.*, 2021, **44**, 3348–3356.
53 N. Kolderová, T. Neveselý, J. Šturala, M. Kuchař, R. Holakovský and M. Kohout, *Chromatographia*, 2017, **80**, 547–557.
54 I. Ali, M. Suhail, L. Asnin and H. Y. Aboul-Enein, *J. Liq. Chromatogr. Relat. Technol.*, 2017, **40**, 435–441.
55 P. Vaňkátová, A. Kubíčková, M. Cigl and K. Kalíková, *J. Supercrit. Fluids*, 2019, **146**, 217–225.